IEEE Access
Multidisciplinary | Rapid Review | Open Access Journal

Received May 19, 2019, accepted May 31, 2019, date of publication June 10, 2019, date of current version July 3, 2019.

Digital Object Identifier 10.1109/ACCESS.2019.2921993

Thermal Analysis of Fifteen-Phase Permanent Magnet Synchronous Motor Under Different Fault Tolerant Operations

ZHI KUANG, SHAOPENG WU, (Senior Member, IEEE), BOCHAO DU, HAO XU, SHUMEI CUI, AND CHING CHUEN CHAN, (Fellow, IEEE)
Department of Electrical Engineering, Harbin Institute of Technology, Harbin 150001, China

Corresponding author: Shumei Cui (cuism@hit.edu.cn)

This work was supported by the National Natural Science Foundation of China, under Grant 51577035.

ABSTRACT In order to not change the space vector pulse width modulation (SVPWM) control strategy during one phase fault, the five-phase six-bridge arm SVPWM fault tolerant control method for fifteen-phase permanent magnet synchronous motor (PMSM) is proposed in this paper, and the thermal stress of fifteen-phase PMSM under different fault-tolerant operations is analyzed. Firstly, the control model of the fifteen-phase PMSM based on three dq axes is established, the generation mode of the SVPWM is analyzed, and the speed and current loop PI regulators of the control system are designed. Secondly, the fault-tolerant control principle of the five-phase six-bridge arm is analyzed and compared with the hysteresis control strategy of equal amplitude and minimum stator loss. Thirdly, the 3D model of the fifteen-phase PMSM is established, the steady-state temperature and the transient temperature rise considering operating conditions under different fault tolerant operations are analyzed, and corresponding temperature rise results of the stator armature windings are compared separately. Finally, the experimental platform is established, the phase current waveforms tested under load conditions confirm the theoretical analysis of five-phase six-bridge arms and hysteresis control, and the test results of steady-state and transient temperature rise confirm the correctness of the simulation prediction.

INDEX TERMS Multiphase PMSM, thermal analysis, fault tolerant control, finite element method.

I. INTRODUCTION

Multiphase motors have become a research hotspot due to their high power density, high reliability and fault tolerance [1], [2], which are widely used in special applications such as ship drive [3], multi-electric aircraft [4]–[6] and other modern AC drives. Multi-phase motors can divide the electric power evenly into the pins of more inverters to reduce the switching current of each device. Moreover, when one or two phases windings are open, the connection mode of the motor is not changed, and the remaining healthy phases can continue to operate. Fault-tolerant operations generally uses appropriate current control strategies to reduce the effects of faults on motor performance, such as torque ripple [7], noise [8], loss [9]. However, when the motor is operating in fault tolerant asymmetric conditions, thermal overload may cause serious damage to temperature-sensitive components, especially the windings insulation system. Previous thermal stress studies have typically focused on motors operation in healthy mode, without considering the fact that fault tolerant control causes a sharp increase in the temperature of some phase windings beyond the thermal constraints of the insulation system. Therefore, the motor designed in healthy mode may not be able to meet the fault operation mode. So thermal analysis plays a more important role for motors used in short-term overload and fault-tolerant operations, such as automotive and aerospace.

In order to maximize the output performance of multi-phase motors in fault tolerance, the modeling of multi-phase motors and the control methods of different topologies are described [10]–[14], the control strategy for dual three-phase PMSM based on reduced order mathematical model under fault condition is analyzed [15], and fault-tolerant control of fifteen-phase induction machine under asymmetrical fault condition is studied [16]. When one or two phases are open circuited, the H-bridge control

The associate editor coordinating the review of this manuscript and approving it for publication was Atif Iqbal.

method is adopted, the current of the open circuit phase is directly divided into the healthy phases to ensure equal output torque [17], this analysis method does not take into account the asymmetrical operation of the current amplitude of the remaining healthy phases under fault tolerant operation. There is also a re-wiring of the output pins of a standard three-phase motor inverter to improve the drive performance [18], the thermal stress of the motor is analyzed when the windings are connected in different combinations [19], [20], but these need to be constantly changing on the hardware according to different combinations, so the above method is not applicable to a high reliability occasion. In this paper, the five-phase six-arm control method is proposed to achieve fault-tolerant control of fifteen-phase PMSM without changing the SVPWM control strategy and adding additional hardware, which helps to improve the operability of the control system during fault-tolerant operation. Compared with the hysteresis control strategy of equal amplitude and stator minimum loss, the current phase and amplitude of each phase winding under normal operation and fault tolerance are analyzed.

The electromagnetic thermal coupling model based on FEM is introduced, and the main influence factors of the maximum thermal behavior during transient operation are analyzed in [21], [22]. The loss distribution under the driving condition cycle [23]–[25] and the equivalent thermal parameters of the windings are introduced into the thermal model [26]. The fastest and maximum temperature rise occurs in the stator armature windings when the motor is operating under overload conditions [27], and different thermal models for short-term thermal transients are proposed [28]–[30]. In summary, the thermal analysis methods are mainly divided into numerical methods and analytical methods. Numerical methods include 2D/3D FEM and computational fluid dynamics (CFD), which can be used in complex areas with high precision, but the amount of calculation is large. In this paper, the lumped parameter thermal network is employed to analyze the thermal stress of fifteen-phase PMSM under normal operation and different fault tolerance conditions. The steady-state temperature of the motor and the transient temperature rise considering the operating conditions are analyzed to obtain the accurate thermal stress inside motor under different control modes.

In this paper, the control model of fifteen-phase PMSM based on three dq axes SVPWM is established in the section II. Hysteresis control and proposed five-phase six-bridge arm SVPWM fault-tolerant control are analyzed in the section III. The simulation analysis based on 3D FEM thermal model of the fifteen-phase PMSM is performed in section IV. The experiment results are tested in section V. The conclusions are discussed in section VI.

II. THE CONTROL MODEL OF FIVETEEN-PHASE PMSM

The stator windings of fifteen phase PMSM is designed as 3*5 phase structure, and the neutral points of the three sets of windings are independent of each other, the spatial

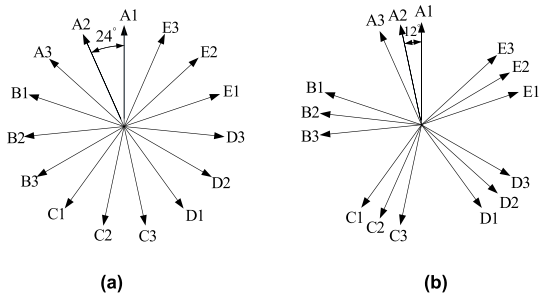

FIGURE 1. Space distribution of fifteen phase PMSM stator winding (a) fully symmetric structure (b) semi symmetric structure.

distribution of its windings is shown in Fig. 1. The spatial phase difference between adjacent windings in each set of five-phase windings is $2\pi/5$ electrical angle, according to the spatial phase difference of the three sets of five-phase windings, the armature windings of the motor are divided into fully symmetrical and semi-symmetrical structures.

The stator voltage and flux linkage equations of a fifteen-phase PMSM are as follows.

$$U_s = R_s I_s + \frac{d\psi_s}{dt} \tag{1}$$

$$\psi_s = L_s I_s + \gamma_s \psi_{fd} \tag{2}$$

where

$$U_s = \left[\, u_{a1}\ u_{b1}\ u_{c1}\ u_{d1}\ u_{e1}\ \cdots\ u_{a3}\ u_{b3}\ u_{c3}\ u_{d3}\ u_{e3} \,\right]^{\mathrm{T}}$$

$$I_s = \left[\, i_{a1}\ i_{b1}\ i_{c1}\ i_{d1}\ i_{e1}\ \cdots\ i_{a3}\ i_{b3}\ i_{c3}\ i_{d3}\ i_{e3} \,\right]^{\mathrm{T}}$$

$$\psi_s = \left[\, \psi_{a1}\ \psi_{b1}\ \psi_{c1}\ \psi_{d1}\ \psi_{e1}\ \cdots\ \psi_{a3}\ \psi_{b3}\ \psi_{c3}\ \psi_{d3}\ \psi_{e3} \,\right]^{\mathrm{T}}$$

$$R_s = diag\left[\, r\ r\ r\ r\ r\ \cdots\ r\ r\ r\ r\ r \,\right]$$

$$\gamma_s = [\cos\theta\ \cos(\theta-\alpha)\ \cos(\theta-2\alpha)\ \cos(\theta-3\alpha)\ \cos(\theta-4\alpha)\ \cdots\cos(\theta-2\alpha-2\beta)\ \cos(\theta-3\alpha-2\beta)\ \cos(\theta-4\alpha-2\beta)\,]^{\mathrm{T}}$$

Ψ_{fd} is the magnetic chain amplitude of permanent magnets in each phase winding, $\alpha = 2\pi/5$ is the electrical angle of the adjacent phase inside the five-phase winding, and β is the electrical angle between two adjacent five-phase windings, generally β is $\pi/15$ or $2\pi/15$. The fifteen-phase motor is divided into three sets of five-phase windings, so there are nine sets of inductors, the stator inductance matrix L_s is as follows.

$$L_s = \begin{bmatrix} L_{s1s1} & L_{s1s2} & L_{s1s3} \\ L_{s2s1} & L_{s2s2} & L_{s2s3} \\ L_{s3s1} & L_{s3s2} & L_{s3s3} \end{bmatrix} \tag{3}$$

where L_{s1s1}, L_{s2s2}, and L_{s3s3} respectively represent the internal self-inductance and mutual inductance of the five-phase windings, L_{s1s2}, L_{s1s3}, L_{s2s1}, L_{s2s3}, L_{s3s1}, and L_{s3s2} are the mutual inductance between the three sets of five-phase windings, respectively, and $L_{s1s2} = L_{s2s1}^T$, $L_{s1s3} = L_{s3s1}^T$, $L_{s2s3} = L_{s3s2}^T$.

Taking the counterclockwise direction as the positive direction, the q1 axis leading the d1 axis in the positive direction of 90° electrical angle, according to the principle that

$$T_{r/s} = \begin{bmatrix} T_{11} & 0 & 0 \\ 0 & T_{22} & 0 \\ 0 & 0 & T_{33} \end{bmatrix} \tag{4}$$

$$T_{ii} = \frac{2}{5}\begin{bmatrix} \cos[\theta-(i-1)\beta] & \cos[\theta-\alpha-(i-1)\beta] & \cos[\theta-2\alpha-(i-1)\beta] & \cos[\theta-3\alpha-(i-1)\beta] & \cos[\theta-4\alpha-(i-1)\beta] \\ -\sin[\theta-(i-1)\beta] & -\sin[\theta-\alpha-(i-1)\beta] & -\sin[\theta-2\alpha-(i-1)\beta] & -\sin[\theta-3\alpha-(i-1)\beta] & -\sin[\theta-4\alpha-(i-1)\beta] \\ \cos 3[\theta-(i-1)\beta] & \cos 3[\theta-\alpha-(i-1)\beta] & \cos 3[\theta-2\alpha-(i-1)\beta] & \cos 3[\theta-3\alpha-(i-1)\beta] & \cos 3[\theta-4\alpha-(i-1)\beta] \\ -\sin 3[\theta-(i-1)\beta] & -\sin 3[\theta-\alpha-(i-1)\beta] & -\sin 3[\theta-2\alpha-(i-1)\beta] & -\sin 3[\theta-3\alpha-(i-1)\beta] & -\sin 3[\theta-4\alpha-(i-1)\beta] \\ 1/2 & 1/2 & 1/2 & 1/2 & 1/2 \end{bmatrix} \tag{5}$$

the transformed synthetic magnetic potential is constant, the transformation matrix of the fifteen-phase windings current from the stationary coordinate system to the three dq coordinate system is as follows (4) and (5), as shown at the top of this page, where i is the serial number of the five-phase winding, and its value is 1, 2, 3, the θ in the T_{ii} matrix is the electrical angle between the reference coordinate axis q and the axis of the stator winding A1, which are rotated by the rotor synchronous rotational speed ω.

In equation (1), both sides are multiplied by the transformation matrix $T_{r/s}$ at the same time, and the equation can be obtained as follows.

$$\begin{aligned} T_{r/s}U_s &= T_{r/s}R_sI_s + T_{r/s}\frac{d\psi_s}{dt} \\ &= (T_{r/s}R_sT_{r/s}^{-1})(T_{r/s}I_s) \\ &\quad + \frac{d(T_{r/s}\psi_s)}{dt} - \left(\frac{dT_{r/s}}{dt}T_{r/s}^{-1}\right)(T_{r/s}\psi_s) \end{aligned} \tag{6}$$

where

$$T_{r/s}U_s = [\,u_{d1}\ u_{q1}\ u_{z11}\ u_{z12}\ u_{o1}\ \cdots\ u_{d3}\ u_{q3}\ u_{z31}\ u_{z32}\ u_{o3}\,]^{\mathrm{T}}$$
$$T_{r/s}I_s = [\,i_{d1}\ i_{q1}\ i_{z11}\ i_{z12}\ i_{o1}\ \cdots\ i_{d3}\ i_{q3}\ i_{z31}\ i_{z32}\ i_{o3}\,]^{\mathrm{T}}$$
$$T_{r/s}\psi_s = [\,\psi_{d1}\ \psi_{q1}\ \psi_{z11}\ \psi_{z12}\ \psi_{o1}\ \cdots\ \psi_{d3}\ \psi_{q3}\ \psi_{z31}\ \psi_{z32}\ \psi_{o3}\,]^{\mathrm{T}}$$

Regardless of the cubic plane harmonics in the coordinate transformation and the zero sequence components in the three sets of windings, the resistance coefficient matrix and the flux chain coefficient matrix are substituted, and the voltage equation can be written as follows.

$$\begin{bmatrix} u_{d1} \\ u_{q1} \\ u_{d2} \\ u_{q2} \\ u_{d3} \\ u_{q3} \end{bmatrix} = \begin{bmatrix} r & 0 & 0 & 0 & 0 & 0 \\ 0 & r & 0 & 0 & 0 & 0 \\ 0 & 0 & r & 0 & 0 & 0 \\ 0 & 0 & 0 & r & 0 & 0 \\ 0 & 0 & 0 & 0 & r & 0 \\ 0 & 0 & 0 & 0 & 0 & r \end{bmatrix} \begin{bmatrix} i_{d1} \\ i_{q1} \\ i_{d2} \\ i_{q2} \\ i_{d3} \\ i_{q3} \end{bmatrix} + \begin{bmatrix} \dot{\psi}_{d1} \\ \dot{\psi}_{q1} \\ \dot{\psi}_{d2} \\ \dot{\psi}_{q2} \\ \dot{\psi}_{d3} \\ \dot{\psi}_{q3} \end{bmatrix}$$
$$+ \omega \begin{bmatrix} 0 & -1 & 0 & 0 & 0 & 0 \\ 1 & 0 & 0 & 0 & 0 & 0 \\ 0 & 0 & 0 & -1 & 0 & 0 \\ 0 & 0 & 1 & 0 & 0 & 0 \\ 0 & 0 & 0 & 0 & 0 & -1 \\ 0 & 0 & 0 & 0 & 1 & 0 \end{bmatrix} \begin{bmatrix} \psi_{d1} \\ \psi_{q1} \\ \psi_{d2} \\ \psi_{q2} \\ \psi_{d3} \\ \psi_{q3} \end{bmatrix} \tag{7}$$

The coordinate transformation of the flux linkage equation in equation (2) is performed, and both sides are multiplied by the transformation matrix $T_{r/s}$ at the same time, and the formula is as follows.

$$\begin{aligned} T_{r/s}\psi_s &= T_{r/s}L_si_s + T_{r/s}\gamma\psi_{fd} \\ &= (T_{r/s}L_sT_{r/s}^{-1})(T_{r/s}i_s) + T_{r/s}\gamma\psi_{fd} \end{aligned} \tag{8}$$

The third-order component of each winding is ignored and the zero-sequence component orthogonal to the direct-axis component of each windings is neglected. The leakage inductance of the mutual inductance between the windings is neglected, and the flux linkage equation is obtained as follows.

$$\begin{bmatrix} \psi_{d1} \\ \psi_{q1} \\ \psi_{d2} \\ \psi_{q2} \\ \psi_{d3} \\ \psi_{q3} \end{bmatrix} = \begin{bmatrix} L_d & 0 & L_{dd} & 0 & L_{dd} & 0 \\ 0 & L_q & 0 & L_{qq} & 0 & L_{qq} \\ L_{dd} & 0 & L_d & 0 & L_{dd} & 0 \\ 0 & L_{qq} & 0 & L_q & 0 & L_{qq} \\ L_{dd} & 0 & L_{dd} & 0 & L_d & 0 \\ 0 & L_{qq} & 0 & L_{qq} & 0 & L_q \end{bmatrix} \begin{bmatrix} i_{d1} \\ i_{q1} \\ i_{d2} \\ i_{q2} \\ i_{d3} \\ i_{q3} \end{bmatrix} + \begin{bmatrix} 1 \\ 0 \\ 1 \\ 0 \\ 1 \\ 0 \end{bmatrix} \psi_{fd} \tag{9}$$

where L_d is the direct axis self-inductance, L_q is the quadrature axis self-inductance, L_{dd} is the mutual inductance between the direct axes of the corresponding windings, L_{qq} is the mutual inductance between the quadrature axes of the corresponding windings.

The electromagnetic torque is derived from the magnetic common energy to the mechanical angle.

$$T_e = \frac{1}{2}i_s^T\frac{\partial L_s}{\partial\theta_m}i_s + i_s^T\frac{\partial\gamma_s}{\partial\theta_m}\psi_{fd} = p_n\left(\frac{1}{2}i_s^T\frac{\partial L_s}{\partial\theta}i_s + i_s^T\frac{\partial\gamma_s}{\partial\theta}\psi_{fd}\right) \tag{10}$$

According to the inductance matrix, the current matrix and the flux matrix, the electromagnetic torque is deduced

as follows.

$$T_e = \frac{5}{2} p_n [(i_{q1}\psi_{d1} - i_{d1}\psi_{q1}) + (i_{q2}\psi_{d2} - i_{d2}\psi_{q2}) + (i_{q3}\psi_{d3} - i_{d3}\psi_{q3})] \quad (11)$$

It can be seen from formula (11) that each set of windings transformation matrix is consistent with a single five-phase motor transformation matrix, and the output electromagnetic torque of the fifteen-phase PMSM is the sum of the torques of the three five-phase windings. However, it is still inaccurate to make the fifteen-phase motor equivalent to three five-phase motors, because the windings of three five-phase motors are coupled on both the direct-axis and the quadrature axis. The fifteen-phase PMSM is controlled according to the rotor field orientation vector. As shown in Fig. 2, the entire control loop consists of a PI speed loop regulator and six PI current loop regulators. The fifteen-phase PMSM is a surface-mount structure, the three sets of windings d-axis currents are given zero during vector control.

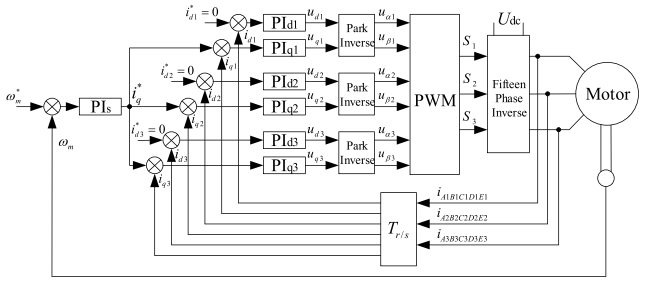

FIGURE 2. Fifteen-phase PMSM SVPWM control based on three dq models.

The three sets of five-phase windings adopt coordinate transformation, which must contain a zero vector and four other degrees of freedom to form the fundamental plane and the third harmonic plane. The (10k±1)th harmonic is distributed in the fundamental plane and (10k±3)th harmonic is distributed in the third harmonic plane, which rotates in the rotor synchronous coordinates at ω and 3ω speeds, respectively. According to the three dq axis coordinate transformation, each five-phase winding generates a separate SVPWM output signal, the voltage vector of each five-phase winding contains thirty non-zero vectors and two zero vectors, and the thirty non-zero vectors have three different amplitudes, the large vector $U_{\max} = 0.6247U_{dc}$, the medium vector $U_{\text{mid}} = 0.4U_{dc}$, and the small vector $U_{\min} = 0.2472U_{dc}$. The voltage vector is distributed in $\alpha_1 - \beta_1$ and $\alpha_3 - \beta_3$ subspace is shown in Fig. 3.

In order to effectively suppress the third harmonic in the five-phase winding, the near four vector (NFV) control method is used to realize the power switch conduction. Define the on-times of the voltage vectors U_{16}, U_{24}, U_{25} and U_{29} as T_1, T_2, T_3, T_4, respectively. When the voltage conduction time meets the following formula (12), the third harmonic in the phase current of the five-phase winding can be effectively

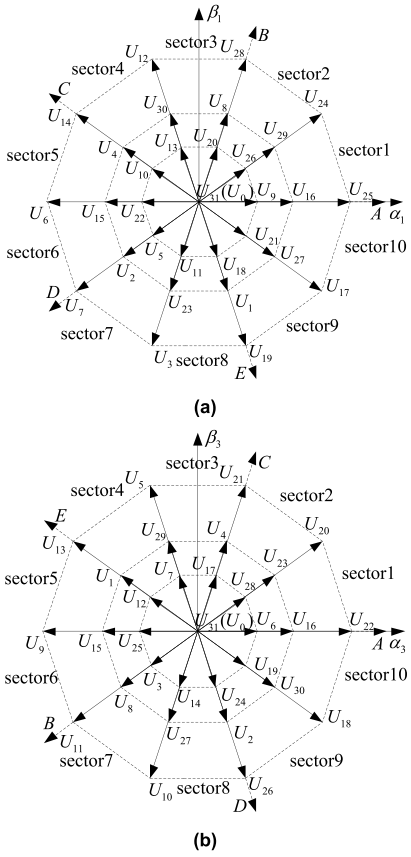

FIGURE 3. Voltage vector distribution (a) $\alpha 1$-$\beta 1$ subspace (b) $\alpha 3$-$\beta 3$ subspace.

suppressed [31].

$$\frac{T_3}{T_1} = \frac{T_2}{T_4} = 1.618 \quad (12)$$

At this time, the ratio of the on-time of U_{25} and U_{16} is equal to the ratio of the on-time of U_{24} and U_{29}, the actual on-time of each voltage vector can be determined by the following formula (13).

$$\begin{cases} T_1 = \dfrac{0.2764\left|\vec{U}_{ref}\right| \sin\left(k * 36^\circ - \gamma\right)}{U_{mid} \sin 36^\circ} T_s \\ T_2 = \dfrac{0.7236\left|\vec{U}_{ref}\right| \sin\left[\gamma - (k-1) * 36^\circ\right]}{U_{\max} \sin 36^\circ} T_s \\ T_3 = \dfrac{0.7236\left|\vec{U}_{ref}\right| \sin\left(k * 36^\circ - \gamma\right)}{U_{mid} \sin 36^\circ} T_s \\ T_4 = \dfrac{0.2764\left|\vec{U}_{ref}\right| \sin\left[\gamma - (k-1) * 36^\circ\right]}{U_{\max} \sin 36^\circ} T_s \\ T_0 = T_s - T_1 - T_2 - T_3 - T_4 \end{cases} \quad (13)$$

where T_s is the switch cycle, k is the sector of the given voltage, γ is the electric angle of the given voltage U_{ref}, T_0 is zero vector conduction time.

In order to reduce the loss of switching time and improve the efficiency of the drive system, each switch can only be

turned on and off once in one carrier cycle. For example, in the first sector, the vector voltage conduction sequence in the half cycle is $U_0 \rightarrow U_{16} \rightarrow U_{24} \rightarrow U_{25} \rightarrow U_{29} \rightarrow U_{31}$, the voltage conduction sequence and the duty cycle of each stage can be expressed as shown in Fig. 4.

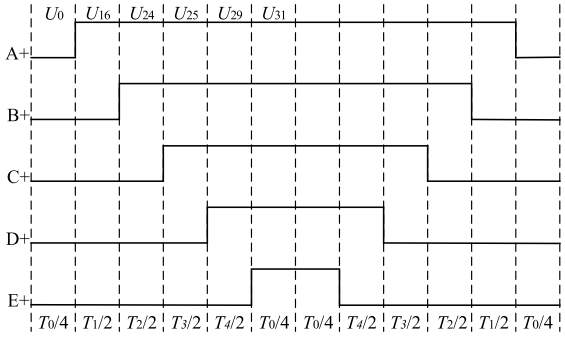

FIGURE 4. PWM output sequence controlled by NFV in the first sector.

The control mode with the direct-axis given zero is applied to the fifteen-phase surface-mount PMSM, only considering the viscous friction of the motor, the equations of motion and electromagnetic torque are as follows:

$$\frac{d\omega_m}{dt} = \frac{1}{J}(T_e - T_L - B_m\omega_m) \tag{14}$$

$$T_e = \frac{15}{2}p_n\psi_r i_q \tag{15}$$

where ω_m is the mechanical angular velocity of rotor, p_n is the number of polar pairs, J is the system moment of inertia, T_L is the electromagnetic torque of motor, is load torque, B_m is the coefficient of viscous friction, ψ_r is the flux of main pole.

The parameters of the three sets of five-phase windings are the same, then the dq-axis voltage equation after the coordinate transformation is as follows.

$$u_d = ri_d + L_d\frac{di_d}{dt} - L_q i_q\omega_r \tag{16}$$

$$u_q = ri_q + L_q\frac{di_q}{dt} + \omega_r L_d i_d + \omega_r\psi_r \tag{17}$$

where ω_r is the electrical angular velocity of rotor, r is armature resistance of stator windings per phase.

In the vector control of the fifteen-phase PMSM, the current of each phase windings is actually controlled by adjusting the dq-axis voltage of the decoupled five-phase windings. According to the formulas (16) and (17), $L_q i_q\omega_r$ and $-(L_d i_d\omega_r + \omega_r\psi_r)$ are added as compensation amounts to the outputs of thedq-axis current PI controllers, respectively, after compensation, the current closed-loop transfer function of dq-axis is shown in Fig. 5.

The transfer function between the voltage and current of the five-phase windings is a first-order inertia link with good stability, Let $k_{pi}/k_{ii} = L_{dq}/r$, then the transfer function $G_c(s)$ of the current negative feedback closed-loop control is as follows.

$$G_c(s) = \frac{G_0(s)}{1 + G_0(s)} = \frac{1}{s(L_{dq}/k_{pi}) + 1} \tag{18}$$

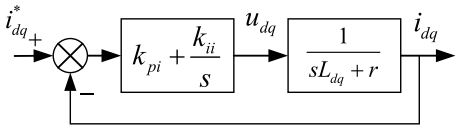

FIGURE 5. The current closed-loop transfer function of dq-axis.

where k_{pi} is the proportional coefficient of PI regulator in current loop, k_{ii} is the integral coefficient of PI regulator in current loop.

The current closed loop is designed as a first order response function, when $s = 0$ is set, the steady state gain of the current closed-loop is 1, and the theoretical steady state error is 0, regardless of the value of k_{pi}. The cutoff frequency of the transfer function satisfies $\omega_{ci} = k_{pi}/L_{dq}$, whose system bandwidth is mainly determined by k_{pi}, but the value of k_{pi} is limited by the maximum DC bus voltage and other protection requirements. Since the d-axis current is given as zero, the system block diagram of the mechanical model of the fifteen-phase PMSM is shown in Fig. 6.

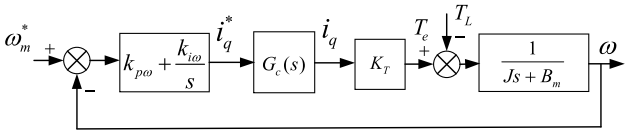

FIGURE 6. The System block diagram of mechanical model of fifteen-phase PMSM.

In order to achieve the speed control of the fifteen-phase PMSM, the system has better response performance and stability, compared with the PI regulator in the speed outer loop, the PI regulator in the current inner loop should have faster response capability. Speed open loop transfer function is as follows.

$$G_{0\omega}(s) = \frac{k_{i\omega}K_T((k_{p\omega}/k_{i\omega})s + 1)}{s(s(L_q/k_{pi}) + 1)(Js + B_m)} \tag{19}$$

where $k_{p\omega}$ is the proportional coefficient of PI regulator in speed loop, $k_{i\omega}$ is the integral coefficient of PI regulator in speed loop, K_T is the proportional coefficient for motor output torque.

The viscous friction coefficient of the motor is generally small, so $B_m \approx 0$. Let $\tau = k_{p\omega}/k_{i\omega}$, $\tau_1 = L_q/k_{pi}$, the transfer function is a type II system, according to the control theory, the shear frequency $\omega_{c\omega}$ of the transfer function $G_{0\omega}(s)$ must be at a slope of -20 dB/dec to make the system stable, so $\tau \gg \tau_1$, the proportional coefficient of the PI regulator in the speed loop satisfies the following equation.

$$k_{p\omega} = \frac{J\omega_{c\omega}}{K_T} \tag{20}$$

In order to ensure the phase angle margin of the system, the proportional integral coefficient of the PI regulator in the speed loop satisfies the following equation.

$$\frac{1}{\tau} = \frac{k_{i\omega}}{k_{p\omega}} \leq \frac{\omega_{c\omega}}{5} \tag{21}$$

According to the basic parameters of the motor, the maximum motor speed $n_{max} = 3000$rpm, the maximum electrical angular velocity $\omega_m = 2\pi n/60$, so the shear frequency $\omega_{c\omega} = 100\pi$(rad/s), the PI regulator parameters of the designed current loop and speed loop are as follows.

$$K_{pi} = 3, \quad k_{ii} = 625.7, \quad k_{p\omega} = 3.36, \quad k_{i\omega} = 218.5$$

III. FAULT-TOLERENT CONTROL MODEL FOR FIVETEEN-PHASE PMSM

The fifteen-phase PMSM adopts 3*5 phase structure distribution, the three neutral points are independent and the control model based on the three dq axes is established. Therefore, when the one phase is open circuited, fault tolerance is performed directly in the five-phase windings of the corresponding open phase. Fault-tolerant SVPWM control strategies are generally implemented using a reduced-order compensated transformation matrix. However, the transformation matrix of the five-phase six-bridge arm SVPWM proposed in this paper remains unchanged before and after fault tolerance. The fault tolerance theory of hysteresis control and proposed method are analyzed below.

A. CURRENT HYSTERESIS FAULT TOLERANT CONTROL

The premise of hysteresis fault-tolerant control is to ensure that the motor's synthetic magnetic potential remains constant before and after an open-circuit fault. Taking the axis of the A1 phase windings as a reference, the composite vector can be converted from a two-dimensional composite space vector to a reference coordinate by a rotation factor. The conversion principle is consistent with the Clark and Park transformations, and the transformation formula is as follows.

$$\frac{5}{2}I_m e^{j\omega t} = i_{a1} + i_{b1}e^{j\alpha} + i_{c1}e^{j2\alpha} + i_{d1}e^{-j2\alpha} + i_{e1}e^{-j\alpha} \tag{22}$$

where I_m is the amplitude of each phase current of the five-phase windings, α is the electrical angle between adjacent windings, which is $2\pi/5$. The equation (22) is developed using the Euler formula, the real part and the imaginary part are equal. The current vector constraint equation as follows.

$$\begin{cases} \frac{5}{2}I_m \cos\omega t = i_{a1} + i_{b1}\cos\alpha + i_{c1}\cos 2\alpha \\ \qquad\qquad + i_{d1}\cos(-2\alpha) + i_{e1}\cos(-\alpha) \\ \frac{5}{2}I_m \sin\omega t = i_{b1}\sin\alpha + i_{c1}\sin 2\alpha \\ \qquad\qquad + i_{d1}\sin(-2\alpha) + i_{e1}\sin(-\alpha) \end{cases} \tag{23}$$

As can be seen from equations (22) and (23), the magnetomotive force space vector formed by the current of a set of five-phase windings operating stably is equivalent to a rotating composite vector with 2.5 times amplitude of the phase current. Therefore, when one phase is open circuited, by adjusting the phase current of five-phase windings, the magnetomotive force vector space of the remaining phase currents is not changed, so the motor can operate with good performance under fault conditions. Assuming that the A1 phase is open, in order to ensure that the currents of the remaining healthy phases are symmetrical to each other and keep the amplitudes equal, the remaining healthy phase current satisfies the formula as follows [32], [33].

$$i'_{b1} = -i'_{d1}, \quad i'_{c1} = -i'_{e1} \tag{24}$$

To meet fault tolerant control with minimum copper loss for one phase open circuit, assuming that the resistance of the stator windings is constant, the copper loss can be replaced by the current function as shown below.

$$I(i'_{b1}, i'_{c1}, i'_{d1}, i'_{e1}) = i'^2_{b1} + i'^2_{c1} + i'^2_{d1} + i'^2_{e1} \tag{25}$$

Since the neutral points of the three sets of windings are independent, the remaining healthy phase current is still satisfied after fault tolerance as follows.

$$i'_{b1} + i'_{c1} + i'_{d1} + i'_{e1} = 0 \tag{26}$$

The magnetomotive force is guaranteed to be constant, and the minimum copper loss of the stator can be transformed into the extreme value problem under the constraint condition. The formula for constructing the Lagrange function with the least copper loss is as follows.

$$\begin{aligned} &F(i'_{b1}, i'_{c1}, i'_{d1}, i'_{e1}, \lambda_1, \lambda_2, \lambda_3) \\ &= (i'^2_{b1} + i'^2_{c1} + i'^2_{d1} + i'^2_{e1}) \\ &\quad + \lambda_1[i'_{b1}\cos\frac{2\pi}{5} + i'_{c1}\cos\frac{4\pi}{5} + i'_{d1}\cos(-\frac{4\pi}{5}) \\ &\quad + i'_{e1}\cos(-\frac{2\pi}{5}) - \frac{5}{2}I_m\cos\theta] \\ &\quad + \lambda_2[i'_{b1}\sin\frac{2\pi}{5} + i'_{c1}\sin\frac{4\pi}{5} + i'_{d1}\sin(-\frac{4\pi}{5}) \\ &\quad + i'_{e1}\sin(-\frac{2\pi}{5}) - \frac{5}{2}I_m\sin\theta] \\ &\quad + \lambda_3(i'_{b1} + i'_{c1} + i'_{d1} + i'_{e1}) \end{aligned} \tag{27}$$

By solving the above formulas (23) and (24), the current amplitude and phase of the remaining healthy windings during equal amplitude fault tolerant control can be obtained. By deriving the partial derivative of the formula (27) and assigning the value to be equal to zero, the current amplitude and phase of the remaining healthy windings with the minimum copper loss can be obtained.

Fault-tolerant control generally equalizes the currents amplitude of the remaining healthy windings or minimizes the copper loss as the control target. The current amplitude and phase of the windings under different fault tolerant targets are shown in TABLE 1.

B. FIVE-PHASE SIX-BRIDGE ARM SVPWM FAULT TOLERANT CONTROL

When one phase is open circuited, in order not to change the implementation of SVPWM under healthy operating, the five-phase six-bridge arm structure is used for fault-tolerant control as shown in Fig. 7. The neutral point of the five-phase windings is taken out and connected to the F1-bridge arm. During healthy operation, the F1-bridge arm does not need to be controlled.

TABLE 1. The current amplitude and phase of the windings under different fault tolerant targets.

Operating status	*Current*	*Five-phase windings*				
		A1	B1	C1	D1	E1
Healthy	Amplitude	1	1	1	1	1
	Phase	0°	72°	144°	-144°	-72°
Equal amplitude (Fault1)	Amplitude	---	1.382	1.382	1.382	1.382
	Phase	---	36°	144°	-144°	-36°
Minimum copper loss (Fault2)	Amplitude	---	1.468	1.263	1.263	1.468
	Phase	---	49.6°	-62.3°	-117.7°	130.4°

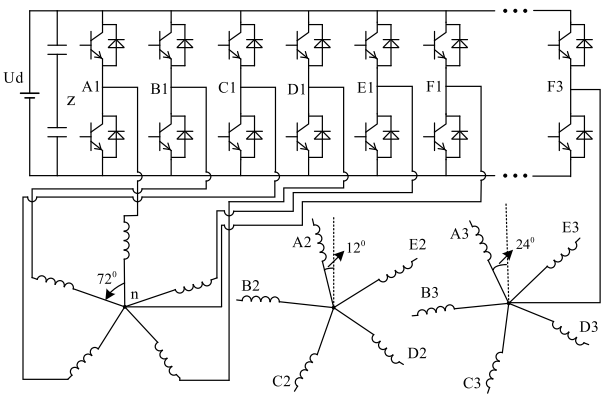

FIGURE 7. The schematic diagram of five-phase six-bridge arm.

Assuming that the A1 phase is open circuited, the F1-bridge arm is controlled by the PWM signal of the healthy operating A1-bridge arm. Since the A1 phase is broken, $U_{A1n} = 0$, $U_{F1z} = U_{A1z}$. The voltage of the remaining healthy phase is as follows.

$$\begin{cases} U_{B1n} = U_{B1z} - U_{nz} = U_{B1z} - U_{A1z} \\ U_{C1n} = U_{C1z} - U_{nz} = U_{C1z} - U_{A1z} \\ U_{D1n} = U_{D1z} - U_{nz} = U_{D1z} - U_{A1z} \\ U_{E1n} = U_{E1z} - U_{nz} = U_{E1z} - U_{A1z} \end{cases} \tag{28}$$

The voltage of each phase of the five-phase windings is multiplied by the rotation factor of the respective spatial distribution. Referring to formula (22), the resultant voltage vector is as follows.

$$\begin{aligned} Us' &= U_{B1n} * e^{j\alpha} + U_{C1n} * e^{j2\alpha} + U_{D1n} * e^{j3\alpha} + U_{E1n} * e^{j4\alpha} \\ &= (U_{B1z} * e^{j\alpha} + U_{C1z} * e^{j2\alpha} + U_{D1z} * e^{j3\alpha} + U_{E1z} * e^{j4\alpha}) \\ &\quad - U_{A1z} * (e^{j\alpha} + e^{j2\alpha} + e^{j3\alpha} + e^{j4\alpha}) \end{aligned} \tag{29}$$

The spatial distribution structure of the five-phase windings is uniformly and symmetrically distributed, and the sum of the rotation factors of each phase is zero.

$$1 + e^{j\alpha} + e^{j2\alpha} + e^{j3\alpha} + e^{j4\alpha} = 0 \tag{30}$$

Formula (30) is substituted into formula (29) and the result is as follows.

$$\begin{aligned} U_s' &= U_{A1z} + U_{B1z} * e^{j\alpha} \\ &\quad + U_{C1z} * e^{j2\alpha} + U_{D1z} * e^{j3\alpha} + U_{E1z} * e^{j4\alpha} = U_s \end{aligned} \tag{31}$$

It can be obtained from formula (31) that the five-phase composite voltage space vector U_s based on the five-phase six-bridge arm control does not change before and after the fault, the five-phase synthetic flux linkage will not change and the trajectory is still circular, so the motor still operating smoothly after one phase windings is open circuited.

Assume that the combined voltage of the five-phase windings is located in the first sector, and its sector is shown in Fig. 3. The SVPWM control strategy of the motor adopts the NFV control operation mode, and the spatially synthesized voltage vector is composed of six voltage space vectors, the conduction sequence is U_0-U_{16}-U_{24}-U_{25}-U_{29}-U_{31}, as shown in Fig. 4. When the motor is running normally, the phase voltage of each phase windings based on the five-phase six-bridge arm SVPWM and $U_{\alpha 1}$, $U_{\beta 1}$, $U_{\alpha 3}$, $U_{\beta 3}$ after coordinate transformation are shown in TABLE 2. When the A1 phase is open, the control strategy based on the five-phase six-bridge arm SVPWM is unchanged, at this time, the phase voltages of the phase windings and $U_{\alpha 1}$, $U_{\beta 1}$, $U_{\alpha 3}$, $U_{\beta 3}$ after coordinate transformation are shown in TABLE 3.

It can be obtained from the comparative analysis of TABLE 2 and TABLE 3, when the A1 phase is open, the SVPWM drive signal of the A1 phase leg is used to drive the F1 phase bridge arm, $U_{\alpha 1}$, $U_{\beta 1}$ and $U_{\alpha 3}$, $U_{\beta 3}$ in the first sector remain unchanged compared with the normal operation. Similarly, $U_{\alpha 1}$, $U_{\beta 1}$ and $U_{\alpha 3}$, $U_{\beta 3}$ of other sectors remain unchanged. Therefore, when the A1 phase is open, it can still be controlled by the normal operation NFV-SVPWM algorithm.

The output electromagnetic torque of the five-phase windings is determined by the magnitude of the direct-axis current i_d and the quadrature-axis current i_q. In order to ensure that the output torque of the five-phase windings is constant, the remaining four phase windings must produce the same i_d and i_q for fault tolerance. Using the inverse Park transformation matrix, the i_d and i_q are converted into i_α and i_β, the inverse Clarke transformation matrix of the five-phase windings is used, the third harmonics are ignored, and the current of the five-phase windings i_{a1}, i_{b1}, i_{c1}, i_{d1}, i_{e1} can be obtained. Because the A1 phase is open, $i_{a1} = 0$, so the neutral point $i_o = -i_\alpha$. For the surface-mount PMSM, the $i_d = 0$ control mode is adopted, and the formula is simplified as follows.

$$\begin{cases} i_{b1} = 1.1756 \sin(\theta + 54^o) i_q \\ i_{c1} = 1.9021 \sin(\theta + 18^o) i_q \\ i_{d1} = 1.9021 \sin(\theta - 18^o) i_q \\ i_{e1} = 1.1756 \sin(\theta - 54^o) i_q \end{cases} \tag{32}$$

It can be seen from the above formula (32) that in order to compensate for the loss of the A1 phase current, the amplitude of the C1 and D1 phase currents increases by 1.902 times,

TABLE 2. The phase voltage based on five-phase six-bridge arm SVPWM during normal operation.

	U_{A1z}	U_{B1n}	U_{C1n}	U_{D1n}	U_{E1n}	$U_{\alpha 1}$	$U_{\beta 1}$	$U_{\alpha 3}$	$U_{\beta 3}$
U_0	0	0	0	0	0	0	0	0	0
U_{16}	$0.8U_d$	$-0.2U_d$	$-0.2U_d$	$-0.2U_d$	$-0.2U_d$	$0.4U_d$	0	$0.4U_d$	0
U_{24}	$0.6U_d$	$0.6U_d$	$-0.4U_d$	$-0.4U_d$	$-0.4U_d$	$0.524U_d$	$0.380U_d$	$0.076U_d$	$-0.235U_d$
U_{25}	$0.4U_d$	$0.4U_d$	$-0.6U_d$	$-0.6U_d$	$0.4U_d$	$0.647U_d$	0	$-0.247U_d$	0
U_{29}	$0.2U_d$	$0.2U_d$	$0.2U_d$	$-0.8U_d$	$0.2U_d$	$0.324U_d$	$0.235U_d$	$-0.124U_d$	$0.380U_d$
U_{31}	0	0	0	0	0	0	0	0	0

TABLE 3. The phase voltages based on five-phase six-bridge arm SVPWM when A1 phase is open.

	$U_{nz(fz)}$	U_{B1n}	U_{C1n}	U_{Dn}	U_{En}	$U_{\alpha 1}$	$U_{\beta 1}$	$U_{\alpha 3}$	$U_{\beta 3}$
U_0	0	0	0	0	0	0	0	0	0
U_{16}	$0.5U_d$	$-U_d$	$-U_d$	$-U_d$	$-U_d$	$0.4U_d$	0	$0.4U_d$	0
U_{24}	$0.5U_d$	0	$-U_d$	$-U_d$	$-U_d$	$0.524U_d$	$0.380U_d$	$0.076U_d$	$-0.235U_d$
U_{25}	$0.5U_d$	0	$-U_d$	$-U_d$	0	$0.647U_d$	0	$-0.247U_d$	0
U_{29}	$0.5U_d$	0	0	$-U_d$	0	$0.324U_d$	$0.235U_d$	$-0.124U_d$	$0.380U_d$
U_{31}	0	0	0	0	0	0	0	0	0

and the amplitudes of the B1 and E1 phase currents increase by 1.1756 times, and the phase difference of the adjacent windings changes. The above formula derives the current constraint equation that satisfies the principle of magnetomotive force invariance, therefore, five-phase six-bridge arm fault tolerance is a special way of constant control of magnetomotive force.

IV. THERMAL MODEL FOR FIFTEEN-PHASE PMSM

Regardless of whether the motor is operating under healthy or fault tolerant conditions, its heat source is still mainly composed of copper loss and iron loss. The copper loss is mainly generated by copper resistance in the stator windings. The core loss is mainly composed of the hysteresis loss and eddy current loss in the permanent magnet and the silicon steel sheet, which is caused by the alternating magnetic field generated by the permanent magnet interacting with the alternating current in the stator windings. The core loss is one of the main sources of heat generation for the motor, the iron loss of the stator core and rotor can be calculated from the widely used Bertotti's iron loss model [34]. The unit mass calculation formula is as follows.

$$P = P_h + P_c + P_e = K_h f B_m^2 + K_c f^2 B_m^2 + K_e f^{1.5} B_m^{1.5} \quad (33)$$

where K_h is the hysteresis core loss coefficient, K_c is the eddy current core loss coefficient,K_e is the other stray core loss coefficient, B_m is the amplitude of the alternating magnetic field in the stator and rotor,f is the alternating current frequency in the stator winding.

The copper loss is mainly caused by the current loss in the copper wire of each phase windings. The copper loss formula of the multiphase motor is as follows.

$$P_{Cu} = \sum_{i=1}^{n} I_i^2 R_i \quad (34)$$

where i is the serial number corresponding to each phase, I_i is the effective value of the current in the corresponding i-phase windings, and R_i is the resistance of the corresponding phase windings.

The eddy current loss of the synchronously rotating permanent magnet is generally small, but the permanent magnet is located inside the motor, and the air gap heat dissipation condition in the stator and rotor part is generally poor, so the smaller loss will also produce a higher temperature distribution, and the commonly used loss formula of volume V is as follows.

$$P_{eddy}(t) = \int_V \frac{\left|\vec{J}_e\right|^2}{\sigma} dV = L \int_S \frac{\left|\vec{J}_e\right|^2}{\sigma} dS \quad (35)$$

where $\vec{J}_e$ is the eddy current density of the permanent magnet, σ is the electrical conductivity of the permanent magnet, S is the eddy current section area of the permanent magnet, and L is the axial length of the permanent magnet.

In this paper, a 28-pole 15kw fifteen-phase PMSM is designed as a research model, the output performance indicators of the fifteen-phase PMSM are as follows:

$P_N = 15\text{kW}$, $U_N = 100\text{V}$, $I_N = 10\text{A}$, $L_d = 0.7\text{mH}$, $L_q = 0.7\text{mH}$, $r = 0.146\Omega$, $P_n = 14$, $T_L = 70\text{Nm}$, $J = 0.01\text{kg}\cdot\text{m}^2$, $n_N = 2000\text{r/min}$, $\psi_r = 0.056\text{Wb}$.

The iron loss of the motor in the stator and rotor, the hysteresis loss and eddy current loss of the permanent magnet, and the copper loss of the stator winding are all obtained by 2D FEM simulation. When the motor operates at rated speed of 2000rpm and rated output torque of 70N, the rotor permanent magnet loss, iron loss and stator copper loss under different control modes are shown in TABLE 4, the different control modes include healthy operation, equal amplitude fault tolerant control(Fault1), minimum copper loss fault tolerant control(Fault2), and SVPWM control of five-phase six-legged arms(Fault3).

TABLE 4. The loss of fifteen-phase PMSM under different control modes.

Different control methods	*Iron loss (W)*	*Permanent magnet loss (W)*	*Copper loss(W)*
Healthy	297.09	70.3	290.4
Fault1	297.58	81.26	341.51
Fault2	297.41	80.81	338.84
Fault3	296.56	86.85	387.2

In order to maintain the same speed and torque as the healthy operation mode, copper loss will increase correspondingly during fault tolerant operation, but the iron loss and the permanent magnet loss increase less. The reason is that the synthetic magnetic potential of the motor is unchanged before and after fault tolerant. The model of the fifteen-phase PMSM is shown in Fig. 8.

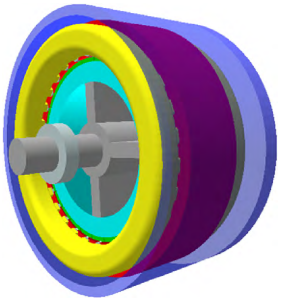

FIGURE 8. The 3d thermal model of fifteen-phase PMSM.

The main concern of this paper is the thermal stress of the motor during healthy operation and fault tolerant operation without derating. The stator and rotor losses of the fifteen-phase PMSM are obtained by 2D finite element simulation. The Finite element thermal analysis is performed in different control modes, where the temperature distribution of the motor is different. On the outer surface of the motor stator, an aluminum cover is added to the model to provide heat dissipation. Therefore, the conduction coefficient during simulation is higher than that of natural air cooling. Considering that the stator silicon steel sheet is not in full contact with the stator shell, there is a very thin equivalent air layer between the stator aluminum shell and the silicon steel sheet in the model. The rotor shaft of the motor has no flux linkage, and the friction loss of the bearing is not considered. All regions of the motor are considered to be homogeneous and isotropic. The conductivity coefficients of various materials in the thermal model of the fifteen-phase PMSM are shown in TABLE 5. There are many turns of copper wire in the stator slot, each conductor surface is insulated, after the winding is successfully completed, it is subjected to dip coating treatment. The equivalent cross-sectional area copper is used in the simulation mode.

TABLE 5. The conductivity coefficients of various materials in the thermal model of fifteen-phase PMSM.

Components	*Thermal conductivity, W/m K*	*Specific heat, J/kg K*	*Density, kg/m^3*
Stator windings	401	385	8933
Stator Lamination	30	460	7650
Slot insulation	0.22	1700	880
Aluminum frame	168	833	2790
Air-gap	0.027	1007	1.127
Permanent magnet	7.6	460	7500
shaft	52	460	7800

The rated load operating point of the motor is selected for analysis, including the temperature distribution of the steady field of the motor during healthy operation and fault tolerant operation. Combined with the operating conditions of all-electric aircraft, the transient temperature rise of the fifteen-phase PMSM during healthy operation and fault tolerant operation also is analyzed.

A. STEADY-STATE TEMPERATURE FIELD

When the fifteen-phase motor is operating at rated load, the copper loss of the stator armature windings and iron loss are the main heat sources, the copper loss of the stator armature windings, the iron loss in the stator and the rotor in TABLE 4 are assigned to the 3D model components in Figure 8. The end of the concentrated windings of the fractional slot is relatively short, and the temperature of the center of the armature windings can be considered to be the highest. The fifteen-phase PMSM adopts three five-phase winding neutral points independent of each other. It is assumed that the A1 phase of the first set of windings is open circuited, fault tolerance control is performed directly in the first set of windings, and the second and third sets of windings operate healthily. When the fifteen phase PMSM operates without derating, the output electromagnetic torque does not change, but the currents in

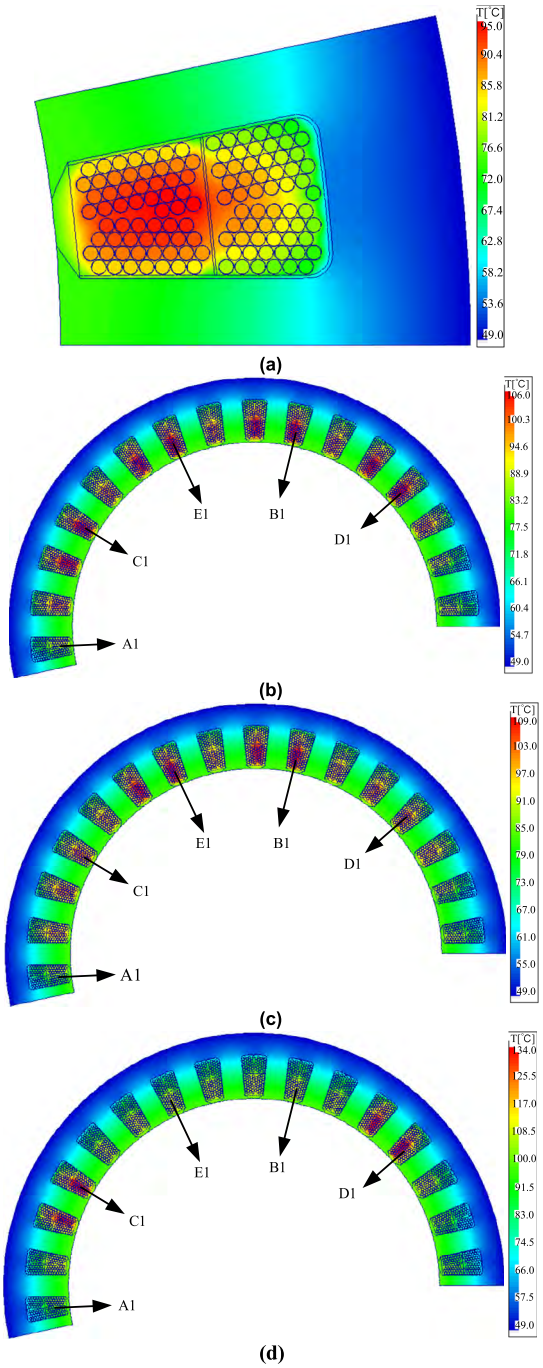

FIGURE 9. The steady-state temperature field distribution of the stator of the fifteen-phase pmsm in different control modes (a) healthy (b) fault1 (c) fault2 (d) fault3.

the first set of windings are not equal due to the fault tolerant operation, then the copper loss is necessarily asymmetrically distributed around the radial direction of the stator windings. The steady-state temperature field distribution of the stator of the fifteen-phase PMSM in healthy operation and the different fault tolerant modes under the rated speed 2000rpm and the rated output load 70N is shown in Fig. 9.

When the fifteen-phase PMSM is operating under healthy operation, the copper loss of the fifteen-phase windings is basically equal, the highest temperature point at the center of the stator windings of the motor is basically the same. When the A1 phase in the first set of windings is open, the current amplitude and phase of each phase windings in the first set of windings change under different fault tolerant operations, while the second set of windings and third set of windings remain in healthy operation.

Different fault tolerant operations of the above-mentioned one phase open circuit are considered, and the temperature distribution cloud diagram are shown in Fig. 5 b), c), d) respectively. The maximum steady-state temperature of windings under different operating modes at rated load and speed are shown in TABLE 6.

TABLE 6. The maximum steady-state temperature of the windings under different operating modes at rated load and speed.

Windings	*Temperature* [°C]			
	Healthy	*Fault1*	*Fault2*	*Fault3*
Phase A1（Slot 1）	95.0	83.1	81.2	81.5
Phase C1（Slot 4）	94.5	105.8	96.2	133.0
Phase E1（Slot 7）	94.0	105.6	109.2	98.6
Phase B1（Slot 11）	95.0	106.0	108.4	98.4
Phase D1（Slot15）	94.6	105.5	96.4	134.0

The fifteen-phase PMSM adopts double-layer windings, a portion of the D3 phase winding is co-located with a portion of the A1 phase winding in a slot, when A1 phase is open, even if the copper loss of the A1 phase windings is zero, however, the temperature in the corresponding slot is still high, because the D3 phase winding is still operating healthily, and the maximum temperature of the winding center of the corresponding slot will be reduced. In the fault-tolerant operation, the slot center of the other two sets of stator windings will exist the highest temperature, but the maximum value will never exceed the value in TABLE 6 and will not be described here. In summary, the steady-state temperature distribution of the above-mentioned slot center is basically consistent with the copper loss distribution of each phase windings in the fault tolerant operation of the theoretical analysis. The steady-state temperature distribution of the windings in the slot verifies the correctness of the theoretical analysis.

B. TRANSIENT TEMPERATURE FIELD

Using the fifteen-phase PMSM to directly drive the propeller, the temperature rise caused by the change of motor speed and torque demand during the whole flight is our main concern. According to the flight condition of a typical two-seater full-electric aircraft [35], the cruising time is shortened, and the required torque and speed are obtained as shown in Fig. 10. Since the output torque of the prototype does not reach the actual operating condition, the output torque of the motor is scaled down according to the torque demanded by the operating conditions. The reduced ratio is the maximum torque

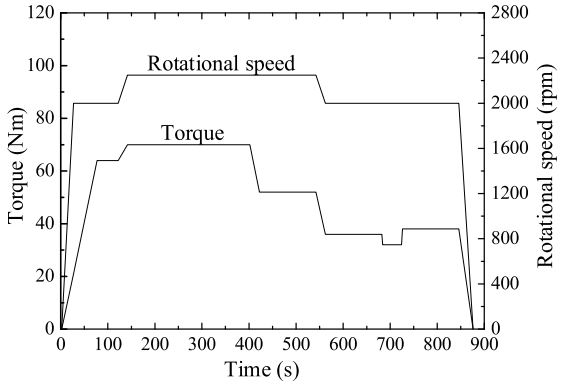

FIGURE 10. The required torque and speed for fifteen-phase PMSM.

required by the actual flight conditions divided by the rated output torque of the motor, and the speed is still changed according to the actual flight conditions.

According to the steady-field temperature distribution results, the corresponding highest temperature points in the windings under different control modes have been found, these highest temperature points of the windings should be the same as the highest temperature point of the windings in the transient temperature rise analysis during flight conditions. The transient temperature changes of the highest temperature rise windings under healthy operation and fault tolerant operation during flight conditions are compared in Fig 11.

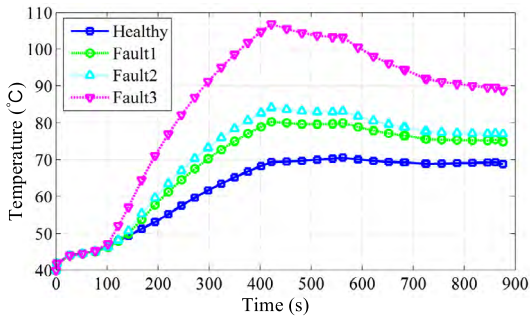

FIGURE 11. The transient temperature rise of the windings in different operating modes under flight conditions.

According to the analysis results of fault tolerance theory and the steady-field temperature distribution results in TABLE 6 in healthy operation, the steady-state temperatures at the slot center of each phase windings are substantially equal. When the A1 phase windings is open circuited and the equal amplitude tolerance control (Fault1) is performed, except that the A1 phase current is zero, the temperature of the slot center corresponding to the four phase windings is substantially equal. When the minimum copper loss tolerant control (Fault2) is performed, the temperature of the slot center corresponding to the B1 and E1 phase windings is the highest. When the five-phase six-bridge arm SVPWM tolerance control (Fault3) is performed, the temperature of the slot center corresponding to C1 and E1 phase windings is the highest. As shown in Fig. 11, under the same operating conditions, the trend of the highest transient temperature rise in the windings under different control modes is basically the same.

V. EXPERIMENTAL RESULTS

The 10kw 28-pole 30-slot fractional slot concentrated windings fifteen-phase surface-mount PMSM is selected as the research object, the temperature sensor PT100 is placed in the center of the motor stator armature windings, and its stator and rotor structure is shown in Fig. 12.

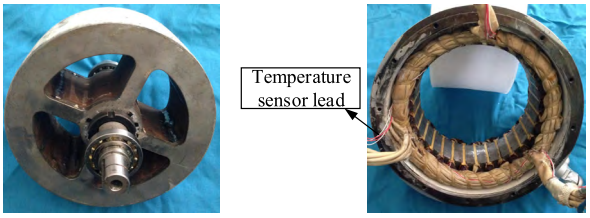

FIGURE 12. The prototype of 30-slot 28-pole surface-mount fifteen-phase PMSM (a) The rotor of motor (b) The stator of motor.

The driving control of the fifteen-phase PMSM requires multiple PWM synchronous outputs, especially for high-power and high-reliability applications. In this paper, the experimental platform based on the combination of DSP and FPGA has been built as shown in Fig. 13. DSP is mainly used for coordinate transformation and space vector control, and FPGA realizes PWM synchronous output. The whole experimental platform is used to verify the three dq axes vector control model of the fifteen-phase PMSM and realize the fault tolerant operation of the five-phase six-bridge SVPWM and current hysteresis.

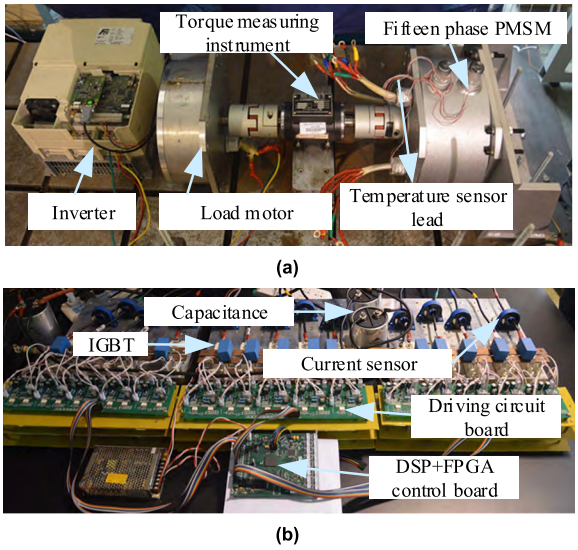

FIGURE 13. Photo of the workbench (a) motor tow platform (b) drive control platform.

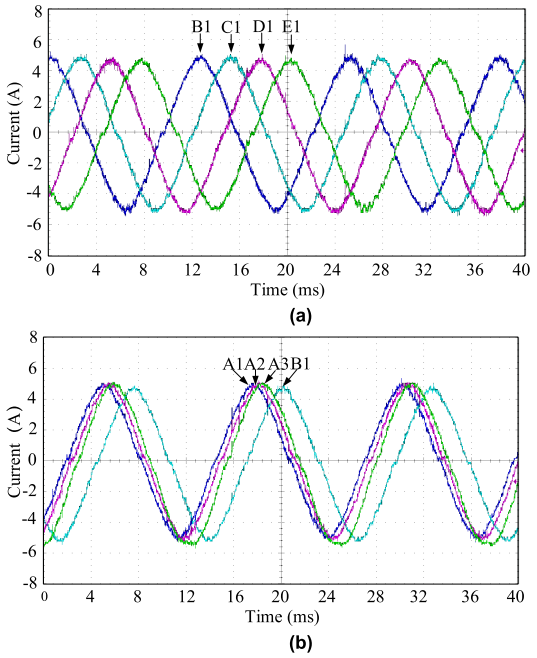

FIGURE 14. The phase current waveform of the fifteen-phase PMSM based on three dq axes SVPWM control. (a) phase current in a five-phase windings (b) phase current between three sets of five-phase windings.

The phase current waveform of the fifteen-phase PMSM based on the SVPWM control of the three dq axes is shown in Fig. 14.

The load torque is 25Nm and the rotational speed is 500rpm, the phase difference of the adjacent phase currents in the five-phase windings is 72°, and the phase difference of the A1, A2, and A3 phases between the three sets is 12°, the experimental test is basically consistent with the theoretical analysis. The experimental results verify that the established vector control model of the three dq axes is feasible.

The load torque is 25Nm and the rotational speed is 500rpm, the fault-tolerant control of the five-phase six-bridge arm SVPWM is used, and the phase current waveform is shown in Fig. 15.

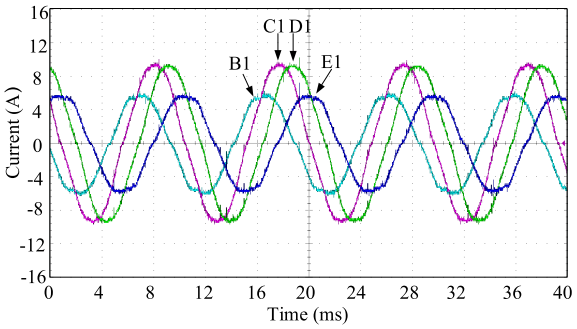

FIGURE 15. The phase current waveform of five-phase six-bridge arm SVPWM fault-tolerant control.

When the A1 phase is open, the fault-tolerant control of the five-phase six-bridge arm is utilized, the amplitude and phase of each phase current of the five-phase windings are basically the same as the theoretical analysis in TABLE 1. The experimental results show that the theoretical analysis of the five-phase six-bridge arm SVPWM fault-tolerant control is correct.

The load torque is 25Nm and the rotational speed is 500rpm, when the A1 phase windings is open, the other two sets of five-phase windings operate normally, and the five-phase winding of the open phase adopts equal amplitude current hysteresis fault-tolerant control, and the phase current waveform is shown in Fig. 16.

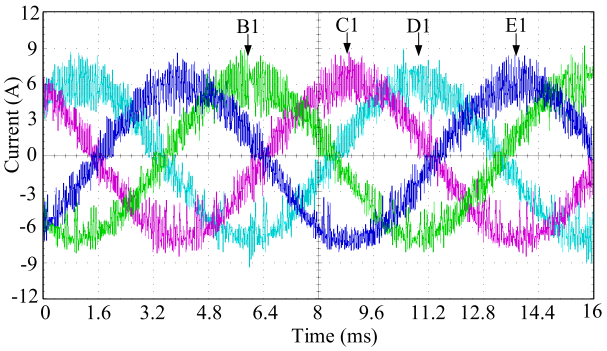

FIGURE 16. The phase current waveform of five-phase windings with current hysteresis fault-tolerant control.

The experimental results show that the amplitude and phase changes of the five-phase windings after fault tolerance are basically consistent with theoretical analysis results of the equal amplitude fault-tolerant control in TABLE 1. The current hysteresis fault-tolerant control can achieve equal-amplitude control of one-phase open circuit, and can also achieve fault-tolerant control of different control targets.

The center of the armature winding of the prototype is placed with the temperature sensor PT100, which is used to measure the internal temperature of the winding when the motor is operating under rated load or different operating conditions. The temperature sensor lead-out line is shown in Figure 13. a). Given a speed of 2000r/min and a load torque of 70N, the center temperature of the armature windings of the fifteen-phase PMSM during healthy operation and different fault tolerant operations is measured, and the temperature rise of the slot center corresponding to the highest temperature are recorded as shown in Fig. 17.

The temperature rise result of the motor armature windings of different control modes under the rated load condition is measured for 90min. The maximum temperature of the armature windings in healthy operation is up to 94.5°, the error compared to the simulated value of the steady-state temperature field is 0.52%. The maximum temperature of the armature windings in equal-amplitude tolerance operation is up to 107.4°, the error compared to the simulated value of the steady-state temperature field is 1.32%. The maximum temperature of the armature windings in minimum copper loss tolerance operation is up to 111.6°, the error compared to the simulated value of the steady-state temperature field

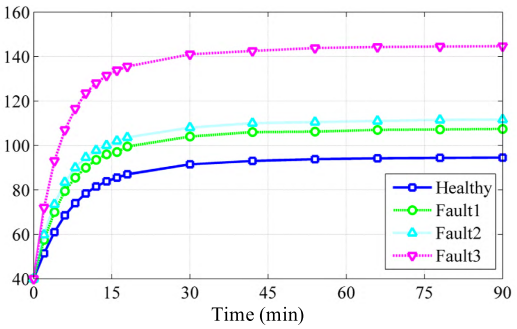

FIGURE 17. The Maximum temperature of armature windings in different operating modes of fifteen-phase PMSM.

is 2.38%. The maximum temperature of the armature windings in five-phase six-bridge arm SVPWM tolerance operation is up to 144.6°, the error compared to the simulated value of the steady-state temperature field is 7.9%. The maximum temperature after stabilization under the rated load is basically the same as the data in TABLE 6, and the experimental data verify the correctness of the theoretical analysis and simulation of the fault tolerance.

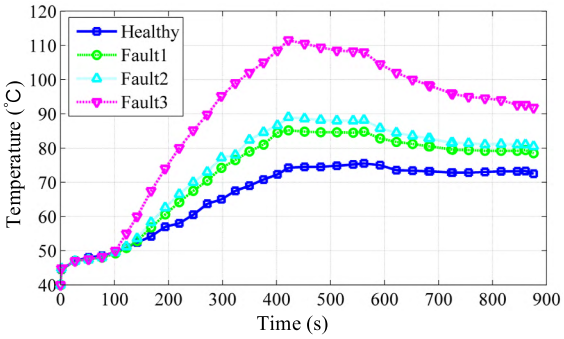

FIGURE 18. The temperature rise variation of armature windings corresponding to the highest temperature under different control operations.

According to the torque and speed requirements shown in Fig. 10, the highest temperature rise of the armature windings under healthy operation and different fault tolerant operation is shown in Fig. 18. The center of the slot of the maximum phase current in the armature winding during healthy operation and fault tolerant operation is the highest temperature point, this result has been verified by the results of steady-state field simulation and experimental data at rated torque and speed output. The fifteen-phase PMSM operates according to the output torque and speed in Fig. 10, the copper loss of the motor armature windings decreases when the torque and speed output decrease at 420s, so the temperature in the armature windings begins to decrease, the change in temperature rise trend is basically consistent with the change in torque output. The simulation results of the temperature rise of the fifteen-phase PMSM during healthy operation and different fault tolerant operation under operating conditions are about 5 degrees lower than the experimental test results, this may be caused by ignoring harmonics during simulation, because the actual operating motor must have harmonic losses due to control errors or structural asymmetry. Since the motor does not operate for a long time at the rated load torque output, the transient temperature does not reach the maximum temperature of the rated steady-state field. Regardless of the mode of operation, the temperature rise of the armature winding of the motor does not exceed the maximum temperature allowed by the insulation level of the armature winding, and the F-stage insulation of the motor windings is used, no more than 155 degrees is considered to be within the allowable range.

VI. CONCLUSION

In this paper, the vector control model based on the three dq axes can effectively realize the motor operation. When fault-tolerant control is applied to the open circuit of one phase windings, except for the windings current of the open circuit is zero, the amplitude and phase of the other four-phase healthy windings current change, and the proposed five-phase six-bridge arm fault tolerance is a special way of constant control of the magnetomotive force. In order to maintain the same torque and speed output as in the healthy mode, the copper loss of the armature windings increases sharply, on the contrary, the iron loss of the motor in the stator and rotor is only slightly increased, the main reason is that the total magnetomotive force of the air gap before and after fault tolerance is constant.

The 3D thermal model of the fifteen-phase PMSM has been built. When the same torque output during normal operation is maintained, the highest temperature point of the armature windings has been found. The steady-state and transient temperature rise of the highest temperature armature windings in healthy operation and different fault tolerant operations are analyzed by finite element analysis and experimental test. When one phase open circuit fault occurs, the temperature rise distribution of the armature windings changes in different fault tolerant modes, but the maximum temperature does not exceed the windings insulation temperature and can continue to operate.

REFERENCES

[1] E. Levi, R. Bojoi, F. Profumo, H. A. Toliyat, and S. Williamson, "Multiphase induction motor drives—A technology status review," *IET Electr. Power Appl.*,, vol. 1, no. 4, pp. 489–516, Jul. 2007.
[2] E. Levi, "Multiphase electric machines for variable-speed applications," *IEEE Trans. Ind. Electron.*, vol. 55, no. 5, pp. 1893–1909, May 2008.
[3] 3M. Benatmane and T. McCoy, "Development of a 19 MW PWM converter for US Navy surface ships," in *Proc. Int. Conf. Electric Ship ELECSHIP*, Istanbul, Turkey, Sep. 1998, pp. 109–113.
[4] M. Villani, M. Tursini, G. Fabri, and L. Castellini, "High reliability permanent magnet brushless motor drive for aircraft application," *IEEE Trans. Ind. Electron.*, vol. 59, no. 5, pp. 2073–2081, May 2012.
[5] W. Cao, B. C. Mecrow, G. J. Atkinson, J. W. Bennett, and D. J. Atkinson, "Overview of electric motor technologies used for more electric aircraft (MEA)," *IEEE Trans. Ind. Electron.*, vol. 59, no. 9, pp. 3523–3531, Sep. 2012.
[6] M. Villani, M. Tursini, G. Fabri, and L. Castellini, "Multi-phase fault tolerant drives for aircraft applications," in *Proc. Elect. Syst. Aircr., Railway Ship Propuls. (ESARS)*, Oct. 2010, pp. 1–6.

[7] T. Gopalarathnam, H. A. Toliyat, and J. C. Moreira, "Multi-phase fault-tolerant brushless DC motor drives," in *Proc. 35th IAS Annu. Meeting World Conf. Ind. Appl. Elect. Energy*, Oct. 2000, pp. 1683–1688.
[8] J. Wang, K. Atallah, and D. Howe, "Optimal torque control of fault-tolerant permanent magnet brushless machines," *IEEE Trans. Magn.*, vol. 39, no. 5, pp. 2962–2964, Sep. 2003.
[9] J. D. Ede, K. Atallah, J. Wang, and D. Howe, "Effect of optimal torque control on rotor loss of fault-tolerant permanent-magnet brushless machines," *IEEE Trans. Magn.*, vol. 38, no. 5, pp. 3291–3293, Sep. 2002.
[10] N. Bianchi, S. Bolognani, and M. D. P. Pre, "Impact of stator winding of a five-phase permanent-magnet motor on postfault operations," *IEEE Trans. Ind. Electron.*, vol. 55, no. 5, pp. 1978–1987, May 2008.
[11] N. Bianchi, S. Bolognani, and M. D. Pre, "Strategies for the fault-tolerant current control of a five-phase permanent-magnet motor," *IEEE Trans. Ind. Appl.*, vol. 43, no. 4, pp. 960–970, Jul. 2007.
[12] F. Baudart, B. Dehez, E. Matagne, D. Telteu-Nedelcu, P. Alexandre, and F. Labrique, "Torque control strategy of polyphase permanent-magnet synchronous machines with minimal controller reconfiguration under open-circuit fault of one phase," *IEEE Trans. Ind. Electron.*, vol. 59, no. 6, pp. 2632–2644, Jun. 2012.
[13] M. J. Duran and F. Barrero, "Recent advances in the design, modeling, and control of multiphase machines—Part II," *IEEE Trans. Ind. Electron.*, vol. 63, no. 1, pp. 459–468, Jan. 2016.
[14] Z. Liu, Y. D. Li, and Z. D. Zheng, "Control and drive techniques for multiphase machines: A review," *Trans. China Electrotech. Soc.*, vol. 32, no. 24, pp. 17–29, 2017.
[15] Z. Changpan, T. Wei, S. X. Dong, Z. Zhaoji, Y. Guijie, and S. Jianyong, "Control strategy for dual three-phase PMSM based on reduced order mathematical model under fault condition due to open phases," *J. Eng.*, vol. 2018, no. 13, pp. 489–494, 2018.
[16] X. Zheng, W. Ma, D. Wang, X. Yi, and H. Liu, "Fault-tolerant control of fifteen-phase induction machine under asymmetrical fault condition," in *Proc. CSEE*, vol. 38, no. 4, pp. 1212–1221, 2018.
[17] N. Bianchi, E. Fornasiero, and S. Bolognani, "Thermal analysis of a five-phase motor under faulty operations," *IEEE Trans. Ind. Appl.*, vol. 49, no. 4, pp. 1531–1538, Jul. 2013.
[18] A. M. S. Mendes, X. M. Lopez-Fernandez, and A. J. M. Cardoso, "Thermal performance of a three-phase induction motor under fault tolerant operating strategies," *IEEE Trans. Power Electron.*, vol. 23, no. 3, pp. 1537–1544, May 2008.
[19] M. Popescu, D. G. Dorrell, L. Alberti, N. Bianchi, D. A. Staton, and D. Hawkins, "Thermal analysis of duplex three-phase induction motor under fault operating conditions," *IEEE Trans. Ind. Appl.*, vol. 49, no. 4, pp. 1523–1530, Jul. 2013.
[20] M. Barcaro, L. Alberti, and N. Bianchi, "Thermal analysis of dual three-phase machines under faulty operations," in *Proc. 8th IEEE Symp. Diagnostics Elect. Mach., Power Electron. Drives*, Sep. 2011, pp. 165–171.
[21] W. Jiang and T. M. Jahns, "Development of efficient electromagnetic-thermal coupled model of electric machines based on finite element analysis," in *Proc. Int. Electr. Mach. Drives Conf.*, May 2013, pp. 816–823.
[22] W. Jiang and T. M. Jahns, "Coupled electromagnetic–thermal analysis of electric machines including transient operation based on finite-element techniques," *IEEE Trans. Ind. Appl.*, vol. 51, no. 2, pp. 1880–1889, Mar./Apr. 2015.
[23] R. Wrobel, D. E. Salt, A. Griffo, N. Simpson, and P. H. Mellor, "Derivation and scaling of AC copper loss in thermal modeling of electrical machines," *IEEE Trans. Ind. Electron.*, vol. 61, no. 8, pp. 4412–4420, Aug. 2014.
[24] X. Wu, R. Wrobel, P. H. Mellor, and C. Zhang, "A computationally efficient PM power loss derivation for surface-mounted brushless AC PM machines," in *Proc. Int. Conf. Electr. Machines (ICEM)*, Sep. 2014, pp. 17–23.
[25] N. Simpson, R. Wrobel, and P. H. Mellor, "Estimation of equivalent thermal parameters of impregnated electrical windings," *IEEE Trans. Ind. Appl.*, vol. 49, no. 6, pp. 2505–2515, Nov. 2013.
[26] T. Chen, X. Wu, Y. Dong, C. Zhang, and H. Liu, "Loss prediction and thermal analysis of surface-mounted brushless AC PM machines for electric vehicle application considering driving duty cycle," *Math. Problems Eng.*, vol. 2016, 2016, Art. no. 8783615.
[27] V. T. Buyukdegirmenci and P. T. Krein, "Induction machine characterization for short-term or momentary stall torque," *IEEE Trans. Ind. Appl.*, vol. 51, no. 3, pp. 2237–2245, May 2015.
[28] A. Boglietti, E. Carpaneto, M. Cossale, and A. L. Borlera, "Stator thermal model for short-time thermal transients," in *Proc. Int. Conf. Electr. Mach. (ICEM)*, Sep. 2014, pp. 1415–1421.
[29] A. Boglietti, E. Carpaneto, M. Cossale, A. L. Borlera, D. Staton, and M. Popescu, "Electrical machine first order short-time thermal transients model: Measurements and parameters evaluation," in *Proc. 40th Annu. Conf. IEEE Ind. Electron. Soc.*, Oct./Nov. 2014, pp. 555–561.
[30] A. Boglietti, E. Carpaneto, M. Cossale, and S. Vaschetto, "Stator-winding thermal models for short-time thermal transients: Definition and validation," *IEEE Trans. Ind. Electron.*, vol. 63, no. 5, pp. 2713–2721, May 2016.
[31] S. Xue and X. Wen, "Novel multiphase SVPWM," *Trans. China Electrotechn. Soc.*, vol. 21, no. 2, pp. 68–72, 2006.
[32] L. Parsa and H. A. Toliyat, "Fault-tolerant five-phase permanent magnet motor drives," in *Proc. IEEE Ind. Appl. Conf., 39th IAS Annu. Meeting.*, Oct. 2004, pp. 1048–1054.
[33] E. Chiricozzi and M. Villani, "Analysis of fault-tolerant five-phase IPM synchronous motor," in *Proc. IEEE Int. Symp. Ind. Electron.*, Jun./Jul. 2008, pp. 759–763.
[34] G. Bertotti, "Space-time correlation properties of the magnetization process and eddy current losses: Theory," *J. Appl. Phys.*, vol. 54, no. 9, pp. 5293–5305, Sep. 1983.
[35] G. Romeo, F. Borello, and G. Correa, "Setup and test flights of all-electric two-seater aeroplane powered by fuel cells," *J. Aircraft*, vol. 48, no. 4, pp. 1331–1341, Jul/Aug. 2011.

ZHI KUANG was born in Hubei Province, China, in 1983. He received the B.S. degree from Taiyuan University of Technology, Taiyuan, in 2006 and master's degree from the Harbin Institute of Technology, Harbin, China, in 2009. He is currently pursuing the Ph.D. degree with the Department of Electrical Engineering, Harbin Institute of Technology, Harbin, China. His research interests include multiphase motor drive, fault tolerance operation, and power electronics.

SHAOPENG WU was born in Heilongjiang, China, in 1983. He received the B.S., M.S., and Ph.D. degrees in electrical engineering from the Harbin Institute of Technology (HIT), Harbin, China, in 2005, 2008, and 2011, respectively.

He was a Visiting Scholar of Wisconsin Electric Machines and Power Electronics Consortium (WEMPEC) with the University of Wisconsin-Madison, Madison WI, USA, from 2013 to 2014. He is currently an Associate Professor with HIT. His current research interests include the design and control of special electric machines, the research of multiphysical coupling, and the related technologies in electromagnetic launch field. Dr. Wu has been a member of the IEEE Magnetics Society and the IEEE Nuclear and Plasma Sciences Society, since 2011. He was a recipient of the Peter J. Kemmey Memorial Scholarship by the 15th International EML Symposium, Brussels, Belgium, in 2010.

BOCHAO DU was born in Heilongjiang Province, China, in 1986. He received the B.S., M.S., and Ph.D. degrees in electrical engineering from the Harbin Institute of Technology (HIT), Harbin, China, in 2009, 2011, and 2016, respectively. He is currently a Lecturer with HIT. His research interests include motor fault diagnosis and fault tolerance operation, motor parameter estimation, power electronics, and motor drivers.

HAO XU was born in Jiangsu Province, China, in 1994. He received the B.S. and M.S. degrees in electrical engineering from the Harbin Institute of Technology (HIT), Harbin, China, in 2016 and 2018, respectively. He is currently an Engineer with China Aero Engine Corporation, Wuxi City, Jiangsu Province, China. His research interests include digital circuit design based on FPGA and DSP, multiphase motor control, and fault tolerance operation.

SHUMEI CUI was born in Heilongjiang, China, on November 22, 1964. She received the Ph.D. degree in electrical engineering from the Harbin Institute of Technology (HIT), Harbin, China, in 1998. She has been a Professor with the Department of Electrical Engineering, HIT. Her research interests include the design and control of micro and special electric machines, electric drive system of electric vehicles, control and simulation of hybrid electric vehicles, and intelligent test and fault diagnostics of electric machines.

He serves as the Vice Director Member of the Micro and Special Electric Machine Committee, and the Chinese Institute of Electronics, and a member of the Electric Vehicle Committee and the National Automotive Standardization Technical Committee.

CHING CHUEN CHAN (F'92) was born in 1937. He received the Ph.D. degree from the University of Hong Kong, in 1982. His work is directly involved in the forefront of electric machines, electric drive, electric vehicles, and smart energy systems. He has made great contributions in building up the fundamental theory of modern electric vehicles and exploring the correlation between energy and information. He proposed many insightful concepts most recently, including smart energy system, energy computer, energy bank, and so forth. He was elected as Academician of Chinese Academy of Engineering and Fellow of the Royal Academy of Engineering U.K., in 1997.